Kovove Mater. 59 2021 21–38
DOI: 10.4149/km_2021_1_21

Influence of aging and annealing processes on the properties of TiB_2 particulate reinforced aluminum composites produced by powder metallurgy

D. Zalaoğlu, M. Übeyli*

Osmaniye Korkut Ata University, Engineering Faculty, Mechanical Engineering, 80000 Osmaniye, Turkey

Received 12 April 2020, received in revised form 19 July 2020, accepted 19 February 2021

Abstract

In this study, the influence of artificial aging at various temperatures and annealing on the mechanical characteristics of the Al-6.2Zn2.3Mg2.3Cu alloy composites bearing various amounts of TiB_2 particulates was investigated. Initially, the composites were produced with the cold pressing aid at 316 MPa and subsequently sintering at 590 ℃. The composites were subjected to artificial aging at 100, 120, and 140 ℃ for 100 hours and the annealing. The microstructural observations were done using the SEM, EDX, and XRD analyses to clarify the materials' phases. Next, the hardness and three-point bending tests of the investigated materials were done. All samples reached their highest hardness values after the artificial aging at 120 ℃ for about 11 h. Besides, the bending strength level of Al-6.2Zn2.3Mg2.3Cu/TiB_{2p} composites was found to be lower than that of the Al-6.2Zn2.3Mg2.3Cu alloy.

K e y w o r d s: metal matrix composites (MMC), powder consolidation, precipitation, hardness test, bending test

1. Introduction

The development of innovative engineering materials opens new windows and presents important opportunities for the advancement of technology and industry. Therefore, manufacturing new materials with superior properties and cost-effective production techniques is strongly required [1–4]. Ceramic particulate reinforced metal matrix composites, having superior properties (i.e., higher strength and modulus, better creep and wear properties) concerning their monolithic counterparts, can exhibit better performance in engineering applications [2–4]. In these materials, types and properties of metal matrix and ceramic reinforcement: features of interface between matrix and ceramic particles, volumetric fraction, distribution, shape, size, and orientation of ceramic particulates, thermal treatment and production methods are essential variables influencing their whole properties [2–4].

Various ceramic materials, such as SiC, Al_2O_3, B_4C, AlN, and TiB_2, can be incorporated into an aluminum or aluminum alloy matrix to enhance mechanical properties to a great extent [5]. Titanium diboride (TiB_2), being one of the hardest ceramics [6–8], is a vital reinforcement candidate to be used in aluminum metal matrix composites [5, 9–62]. The techniques used to fabricate TiB_2 particle reinforced Al composites are salt-metal reaction [9–37], mechanical alloying and sintering [38–42], hot extrusion after mechanical alloying [43], stir casting [44, 45], casting [46, 47], squeeze casting [48], accumulative roll bonding [49], vacuum infiltration [50], hot isostatic pressing [51, 52], pressure infiltration [53], reactive hot pressing [54], hot pressing [55], cold isostatic pressing and sintering [56], cold pressing and hot extrusion [57], and cold pressing and sintering [58–62].

Sadeghian et al. [39] fabricated the Al-TiB_2 nanocomposites by hot extrusion after the spark plasma

*Corresponding author: tel.: +90 328 8271000-3450; e-mail address: mubeyli@gmail.com

sintering of the mechanically alloyed element powders: Ti, Al, and B to prevent the existence of detrimental phases such as Al_3Ti. After the hot extrusion, they measured the mean grain sizes of aluminum and TiB_2 smaller than 100 nm. Besides, they obtained high hardness (180 Vickers hardness) and tensile strength (540 MPa) values for the hot extruded nano-composite due to the mainly nano-scale grains of matrix and reinforcement materials as well as the absence of unwanted intermetallic products during the whole operation period [39].

In another work conducted by Balci et al. [38], an aluminum matrix composite reinforced by TiB_2 was manufactured using cold compaction and successive sintering processes after the mechanical alloying of the Al and TiB_2 powders. They performed microhardness and wear tests for these composites containing various amounts and particle sizes of TiB_2. It was found that the Al composite reinforced with 15 wt.% micron-sized TiB_2 exhibited better wear resistance compared to that reinforced with submicron one. Furthermore, the Al_3Ti compound was detected in the sintered samples at a low scale [38].

Sadeghian et al. [40] produced an aluminum composite reinforced with 20 wt.% TiB_2 by mechanical alloying technique. They applied two steps during the alloying processing of powders: Al, Ti, and B to provide the composite powder free from brittle intermetallic phases, namely titanium aluminides, which are harmful to some mechanical properties [52, 54]. It was stated that there were no intermetallic phases detected in the composite powder after the process [40].

Tjong and Tam [52] manufactured the Al-TiB_2 composites using hot isostatic pressing of the compacted powders consisting of pure Al with different particle sizes and TiB_2 to achieve full densification and avoid the harmful phase formation. They investigated the tensile, thermal expansion, and thermal cycling properties as well as the impact of the particulate size ratio of Al/TiB_2 on the densification of the composite. They found a moderate increment for the tensile strength of composite (from 148 to 191 MPa) when the TiB_2 reinforcement content was increased from 5 to 20 vol.% [52].

In a recent study by Akbari [44], the stir-casting process at 750, 800, and 900 ℃ was applied to produce A356 aluminum alloy composites with different amounts of micro or nano TiB_2 particles (up to 5 vol.%). After the casting, the composites, solutionized at 520 ℃, were artificially aged at 180 ℃. It was pointed out that the porosity level rose with the TiB_2 fraction, and the highest hardness value of 120 Brinell hardness was found for the composite having 1.5 % nano TiB_2 [44].

Paidpilli et al. [58] examined the influence of reinforcement content and the alloy powder type (premixed and prealloyed) on the mechanical and electrical behavior of AA6061/TiB_2 composites that were fabricated via cold compaction and sintering route [58]. In a more recent study [62], the impact of precipitation hardening on some properties of AA2024/TiB_2 composites manufactured by powder metallurgy was examined [62].

According to our literature survey, although numerous studies related to the fabrication of Al-TiB_2 composites, particularly with the aid of in situ salt-metal reaction [9–37] exist, the works conducted on their production using the cold pressing and sintering route are very rare [58–62]. Also, the works concerning the influence of artificial aging on the mechanical behavior of cold-pressed and sintered Al-TiB_2 composites are very limited [59, 61, 62]. The powder metallurgy method has certain advantages compared to casting techniques in the manufacturing of metal matrix composites [2, 51, 63, 64]. It enables more uniform particle distribution and homogeneity throughout the matrix [2, 51, 63, 64]. And also, unwanted reactions and harmful phase formations can be eliminated with the powder metallurgy technique due to the utilization of lower processing temperatures [2, 51, 63, 64].

This research presents the effects of aging and annealing applications on the mechanical and microstructural characteristics of the aluminum composites (Al-Zn-Cu-Mg/TiB_{2p}) reinforced with TiB_2 particulates and manufactured using powder metallurgy. The Al-Zn-Mg-Cu alloys exhibit exceptional mechanical properties owing to their superior age hardening capability [65]. Therefore, these alloys are utilized extensively in crucial fields of industry, such as automotive and aerospace [65]. Initially, the characterization and compressibility behavior of powders were determined. And then, the composites with various TiB_2 particle content were manufactured via cold pressing and sintering technique. After the production, the sinterability of these composites was measured. Next, the artificial aging treatments at different temperatures were applied to the composite samples for 100 h. Finally, the microstructural examinations and mechanical characterizations of the composites were done to see the role of TiB_2 fraction and aging.

2. Experimental procedure

2.1. Powder characterization

At the beginning of the current study, the powders of Al, Zn, Cu, Mg, and TiB_2 with high purity were supplied from the market. And then, their sizes and shapes were specified by a particle size analyzer (Malvern Mastersizer 2000) and the FEI Quanta 650 FEG scanning electron microscope (SEM), successively.

2.2. Mixing and compaction of powders

After the powders' characterization, they were admixed in the Turbula T2F mixer for 2 h to get uniform powder compositions to be cold-pressed. The Al-6.2Zn2.3Mg2.3Cu aluminum alloy (AA) with a nominal composition of 6.2 % Zn, 2.3 % Mg, and 2.3 % Cu in weight and the TiB_2 ceramic in the form of particulates were chosen to be the matrix and reinforcement, successively. The four sample types were taken into account concerning the TiB_{2p} volume fraction changing from 0 to 15 %. The codes were defined to be AA, AA-5TiB_2, AA-10TiB_2, and AA-15TiB_2 for the investigated materials consisting of 0, 5, 10, and 15 vol.% TiB_2, respectively. No binder was used during the powder processing. The mixtures of powders were compacted in a cold mold at different pressures up to 800 MPa to have their compaction pressure (P) vs relative density (D) relations. The compressibility behavior of powder mixtures was investigated by applying the linear regression analysis for the widely used powder compaction models [66–68]. Heckel [66] proposed the below equation for the compressed powders, in which C_1 and C_2 are constants:

$$\ln\left(\frac{1}{1-D}\right) = C_1 P + C_2. \tag{1}$$

Moreover, another equation given below was suggested by Ge [67]:

$$\log\left[\ln\frac{1}{(1-D)}\right] = C_3 \log P + C_4. \tag{2}$$

In this formulation, C_3 and C_4 are also constants [67]. In a more recent study conducted by Panelli and Ambrozio Filho [68], a novel expression for the consolidation behavior of compacted powders was developed to get more precise fittings with the experimental data. This equation is given as follows:

$$\ln\left(\frac{1}{1-D}\right) = C_5\sqrt{P} + C_6, \tag{3}$$

where C_5 and C_6 are constants [68].

In the Eqs. (1)–(3), the constants C_1, C_3, and C_5 reflect the plastic deformation ability of powders during compression whereas, the other constants C_2, C_4, and C_6 represent the apparent density of powders [66–68]. Panelli and Ambrozio Filho [69] applied the linear regression analysis for the experimental results to check the validity of these compaction equations. The details can be found in [69].

2.3. Sintering

The green samples, compressed at 316 MPa, were sintered at 590 ℃ for 15 min with a heating rate of 15 ℃ min^{-1} in a furnace using pure argon atmosphere. The sintering temperature was chosen to be higher than the solidus temperature of the Al-6.2Zn2.3Mg2.3Cu alloy to improve densification [65]. Upon completing the sintering operation, the sinterability of the samples was determined using their green and sintered densities. The sinterability (ϕ), also called densification, can be expressed as below [70]:

$$\phi = \frac{\rho_s - \rho_g}{1 - \rho_g}, \tag{4}$$

where ρ_s and ρ_g are relative densities of sintered and compacted parts, relatively [70]. All the densities were measured using the Archimedes' principle [71], while the theoretical densities were computed with the rule of mixture [2–4]. The porosity content and relative density of the investigated materials were computed.

2.4. Heat treatment

The artificial aging treatments were applied to the fabricated samples to get the hardness-aging time profiles. Firstly, in these treatments, all the investigated materials were held at 480 ℃ in the furnace for 45 min to be solutionized. Then, a subsequent water-quenching was applied to them promptly to finalize the solutionizing procedure. Secondly, they were soaked into an oil bath at 100, 120, and 140 ℃ for the time extending to 100 hours to catch the peak aging points. At certain time intervals, along with the total aging time, the samples were water-quenched to make the Brinell hardness measurements [72]. Thirdly, their aging curves showing hardness versus aging time were constituted. In addition to the aging treatment, the annealing treatment was also facilitated in a chamber furnace for a group of samples to make a comparison. In this treatment, they were held at 420 ℃ for 2 h. After that, their slow cooling was allowed in the furnace.

2.5. Microstructural characterization

Some selected samples, representing the four groups, were subjected to standard metallographic treatment: cutting, grinding, polishing, and etching [73]. The modified Keller's reagent was utilized in the etching step to get the samples ready for the microstructural characterization [73]. After that, the microstructural examinations on the selected samples were done using the SEM (FEI Nova NanoSEM 430). The analyses of the Energy Dispersive X-ray (EDX) and Back Scattered Electron (BSE) on some samples were also made with the aid of the SEM (FEI Quanta 650 FEG). The phases formed within the samples were investigated with the X-Ray Diffractometer (PANalytical EMPYREAN) aid, having Cu K_α radiation of 1.5406 Å wavelength and working at 45 kV and 40 mA.

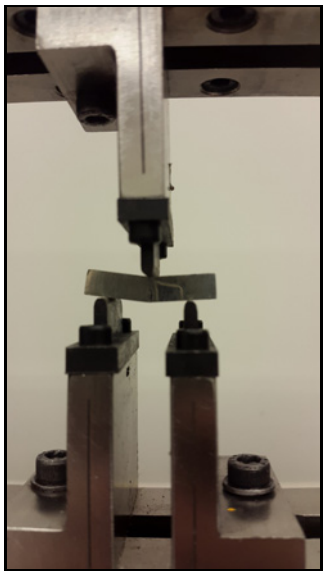

Fig. 1. The three-point bending testing of the composite sample.

The X-Ray Diffraction (XRD) analyses of the investigated materials either in the peak-aged at 120 ℃ or annealed conditions were carried out by scanning the 2θ interval of 10°–90°. The scanning rate was adjusted to be $0.04° \, s^{-1}$. The data gained during the XRD analyses were evaluated with the software HighScore plus [74, 75] utilizing the ICSD database [76].

2.6. Mechanical characterization

The Brinell hardness tests were conducted using the standard ASTM E10-17 [72] to clarify the samples' hardness variation concerning aging temperature and time. Five measurements by exerting the load of 62.5 kg were taken at different locations for each sample to get mean hardness values. Furthermore, according to TS 4222 EN ISO 3325 [77], the three-point bending tests were made for the peak aged and annealed samples. These experiments were made using a tensile testing machine (Instron 3300). The three--point bending testing of the composite sample is exhibited in Fig. 1.

3. Results and discussion

3.1. Powder properties

Table 1 epitomizes the important parameters of the powders (Al, Zn, Cu, Mg, and TiB_2) derived from the particle size analyses. The mean particle size for TiB_2 is 16 μm while that for Al is 11 μm. On the other hand, the mean particle sizes are recorded to be 73, 124, and 62 μm for the Zn, Mg, and Cu powders, successively.

Table 1. The main powder size indicators for the components

Powder	D_{10} (μm)	D_{50} (μm)	D_{90} (μm)
Al	5.18	10.91	22.84
Zn	23.55	72.95	154.62
Mg	55.40	124.10	217.42
Cu	36.46	61.80	94.97
TiB_2	8.60	15.81	29.29

The range between D_{10} and D_{90} for aluminum and titanium diboride powders is found to be relatively narrow.

The SEM pictures of the powders are illustrated in Fig. 2. It is observed that the aluminum powder has a mostly irregular and rounded shape and some rod-like appearance. The copper powder is spherical with some satellite formations, whereas the magnesium and zinc powders have a round morphology. Moreover, the shape of titanium diboride powder looks flakey.

3.2. Compressibility and sinterability of powders

The relative density variations of the materials concerning the compaction pressure are illustrated in Fig. 3. A linear increase of the relative densities with the pressure up to 150 MPa is seen apparently. This increment takes place more slowly and becomes nearly stationary at higher pressures. The highest green density values are reached at ∼ 600 MPa, and there is no more densification up to 800 MPa practically. One can observe from Fig. 3 that the incorporation of TiB_2 particulates diminishes the compressibility of alloy powder remarkably. After the compaction process, the highest relative density for the unreinforced aluminum alloy reaches 0.972, whereas it reduces to 0.965, 0.958, and 0.946 for the composites reinforced with 5, 10, and 15 % TiB_2, respectively.

In the pressing of powders, the particles' movement initially exists to change their settlement by sliding with some local deformation [78–83]. It commences the packing of loose powders by reducing the porosity at a low level. After that, the ductile metal powders begin to be deformed plastically together with the elastic deformation of brittle TiB_2 particles upon increasing the pressure [78–83]. For this reason, the linearly steep rise in the relative density up to intermediate pressure levels (i.e., 150 MPa) obtained in this study is related to this mechanism. The hardening of aluminum particles by cold working entails a deceleration of density rising at higher pressures [78–83]. The brittle titanium diboride particles diminish the plastic deformation of matrix powders either by restricting their rearrange-

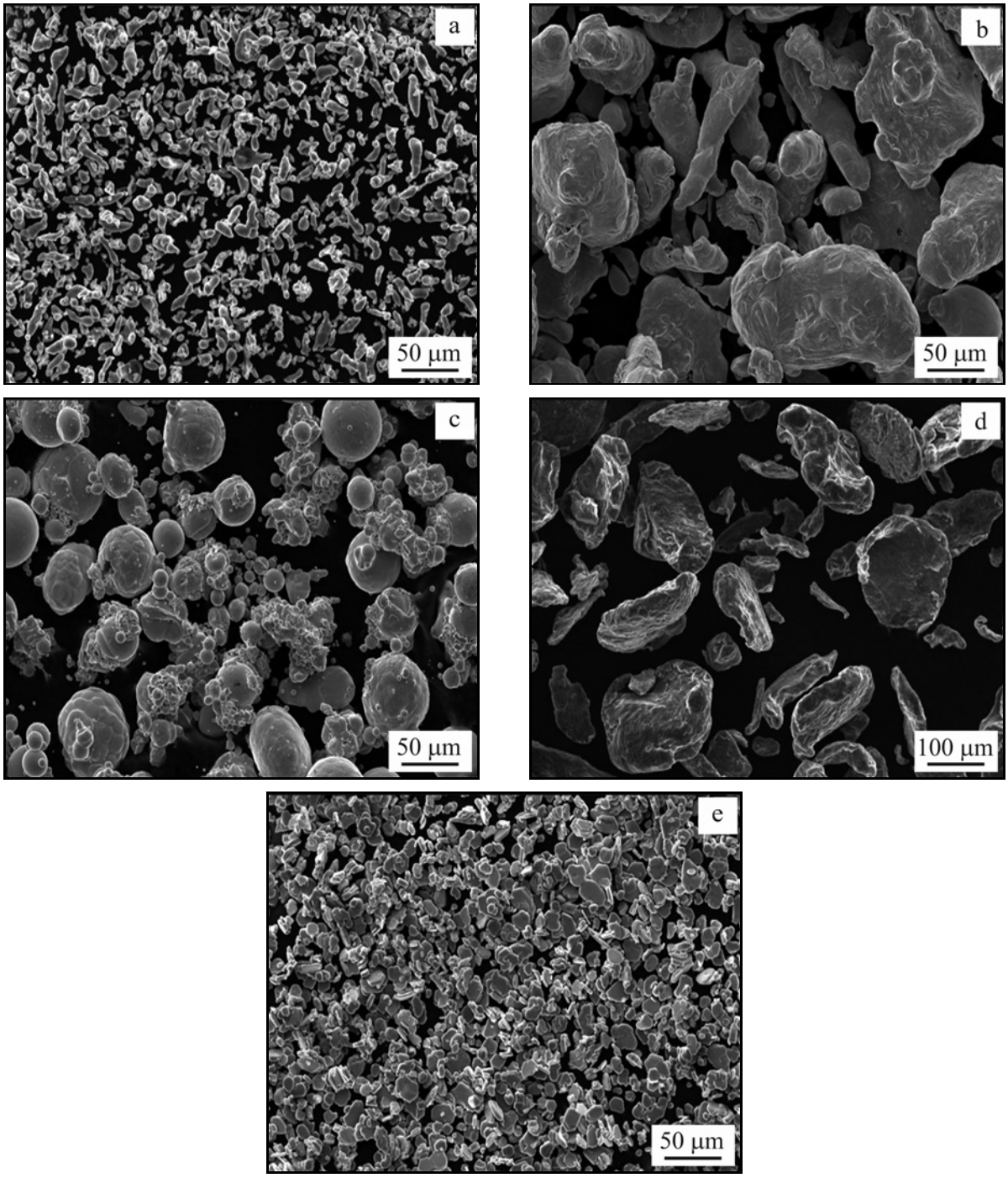

Fig 2. The SEM pictures of powders (a) Al, (b) Zn, (c) Cu, (d) Mg, and (e) TiB_2.

ment for densification or by sharing the compressive load elastically [78–83]. Hence, the lower relative densities are found for the composite samples.

The compressibility behavior of powders, analyzed by the equations of Heckel [66], Ge [67], and Panelli and Ambrozio Filho [68], is depicted in Figs. 4–6, respectively. Table 2 gives the coefficients of linear correlation (R^2) and the constants reflecting the plastic deformation ability of powders for the applied models [66–68]. It can be stated that the linear correlation coefficients are found generally greater than 0.99 in the composite samples for the models of Ge [67] and Panelli and Ambrozio Filho [68]. However, the R^2 values vary between 0.95 and 0.96 for the compacted powder mixtures at different pressures by the Heckel model [66]. Hence, the linear fittings of the experimental data concerning the Ge [67] and Panelli-Ambrozio Filho [68] powder consolidation models are more suited. These compaction relations demonstrated an exact approximation, especially in determining the relative

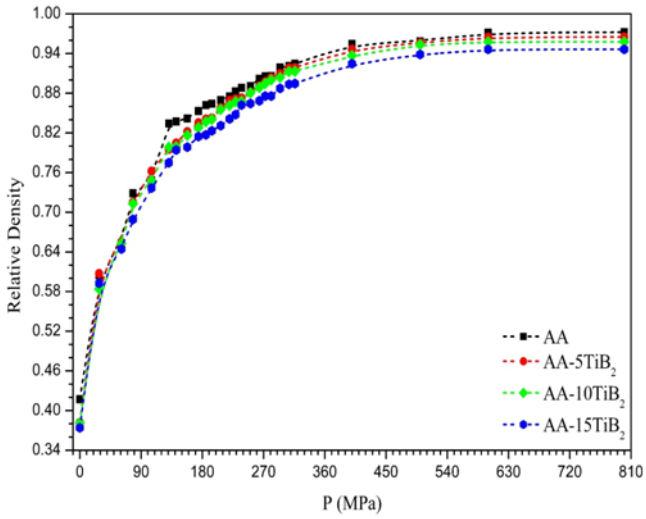

Fig. 3. Compressibility behavior of the investigated composites and the unreinforced alloy.

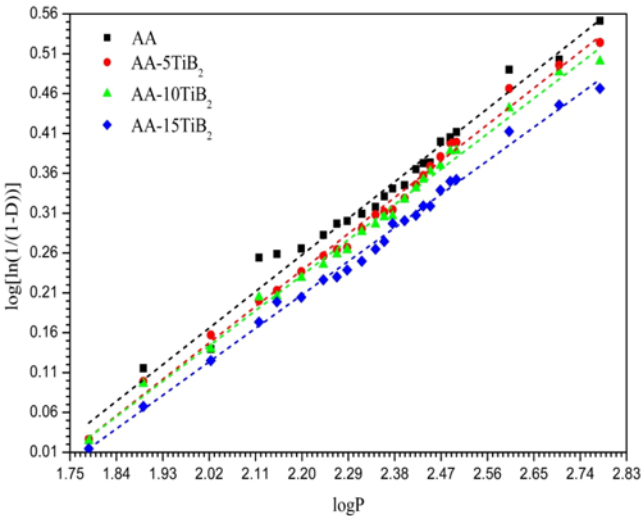

Fig. 5. Consolidation of the investigated powder mixtures by the Ge equation [67].

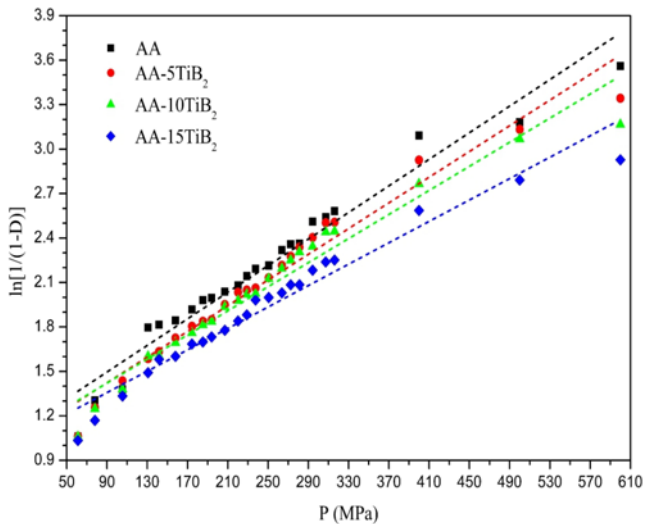

Fig. 4. Densification of the investigated powder mixtures by the Heckel equation [66].

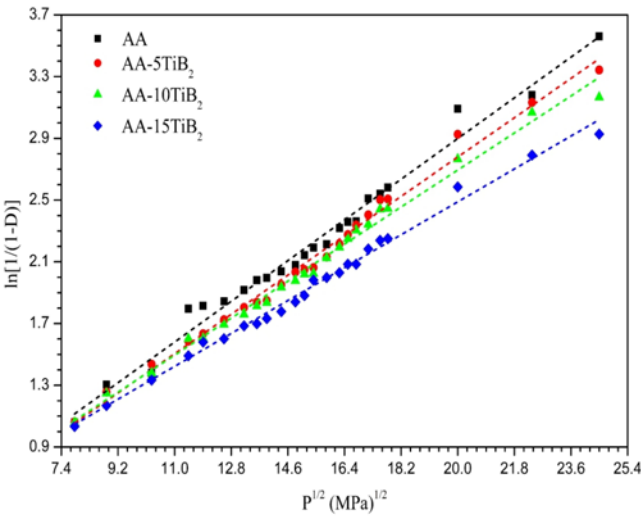

Fig. 6. Densification profile of the investigated powder mixtures by the Panelli and Ambrozio Filho equation [68].

density of compacted powders. The constants C_1, C_3, and C_5, indicating the plastic deformation capability of the compacted powder [78–83], decrease with increasing TiB_2 particulates in the composite pow-

Table 2. The correlation coefficients and the constants of the investigated materials computed using the powder compaction models [66–68]

Samples	Heckel [66]		Panelli and Ambrozio Filho [68]		Ge [67]	
	C_1 (MPa^{-1})	R^2	C_5 (MPa$^{-0.5}$)	R^2	C_3 (MPa^{-1})	R^2
AA	0.00449	0.9553	0.1465	0.9845	0.5098	0.9825
AA-5TiB_2	0.00434	0.9633	0.1415	0.9911	0.5072	0.9929
AA-10TiB_2	0.00406	0.9537	0.1333	0.9915	0.4929	0.9936
AA-15TiB_2	0.00361	0.9547	0.1184	0.9926	0.4670	0.9946

Table 3. Density, sinterability, and porosity of the investigated materials

Sample	Green density ($g\,cm^{-3}$)	Sintered density ($g\,cm^{-3}$)	Theoretical density ($g\,cm^{-3}$)	Sinterability	% Porosity (after sintering)
AA	2.604	2.682	2.817	0.366	4.79
AA-5TiB_2	2.665	2.730	2.901	0.275	5.89
AA-10TiB_2	2.727	2.790	2.986	0.243	6.56
AA-15TiB_2	2.747	2.820	3.070	0.226	8.14

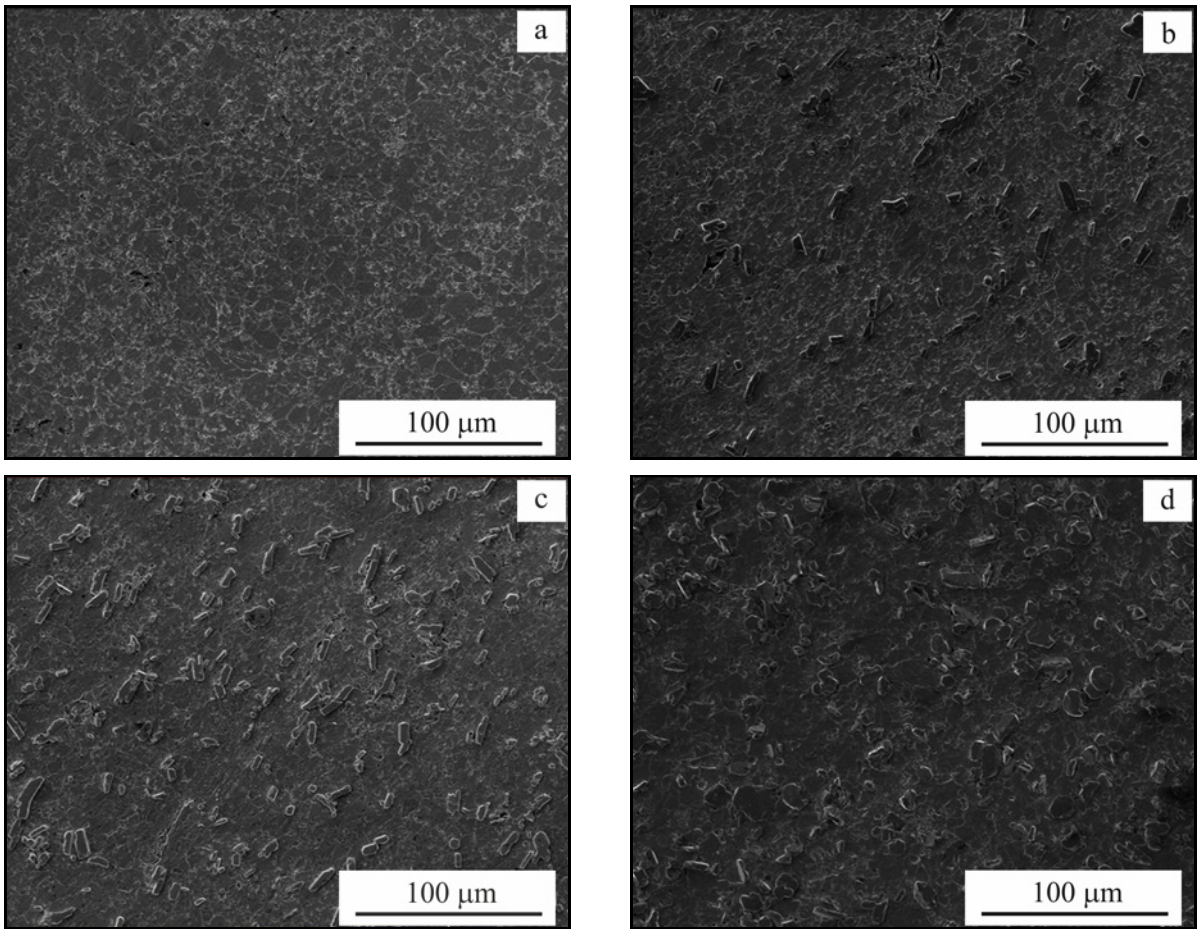

Fig. 7. Typical microstructures of the materials peak aged at 120 ℃: (a) AA, (b) AA-5TiB_2, (c) AA-10TiB_2, and (d) AA-15TiB_2 (1000 ×).

ders. This means that the deformation capability of the alloy particles is constricted by the TiB_2 particles [78–83]. The partition of the applied load between the metal matrix and TiB_2 particulates constrains the plastic deformation of aluminum alloy matrix [78–83].

Table 3 gives the density, porosity, and sinterability of the composites. A gradual decline in both the green and sintered density with an increase in the TiB_2 ratio is observed. The densification of the compacted powder is promoted in the sintering process. The porosity level of the unreinforced aluminum alloy is obtained to be $\sim 4.8\,\%$, whereas it increases with the incorporation of TiB_2 content gradually.

3.3. Microstructural examination

Figure 7 represents the SEM images of the investigated materials, which were peak-aged at 120 ℃. The porosities as black round points are seen apparently in Fig. 7. They are generally formed at the boundaries of the equiaxed grains in the matrix aluminum alloy. Although some local agglomerations of the ceramic particles were recorded, particularly for the composites with 10 or 15 % TiB_2, the dispersion of TiB_2 particles is generally found to be uniform throughout the matrix. The maps of alloying elements throughout the matrix are shown in Fig. 8 for the selected sample,

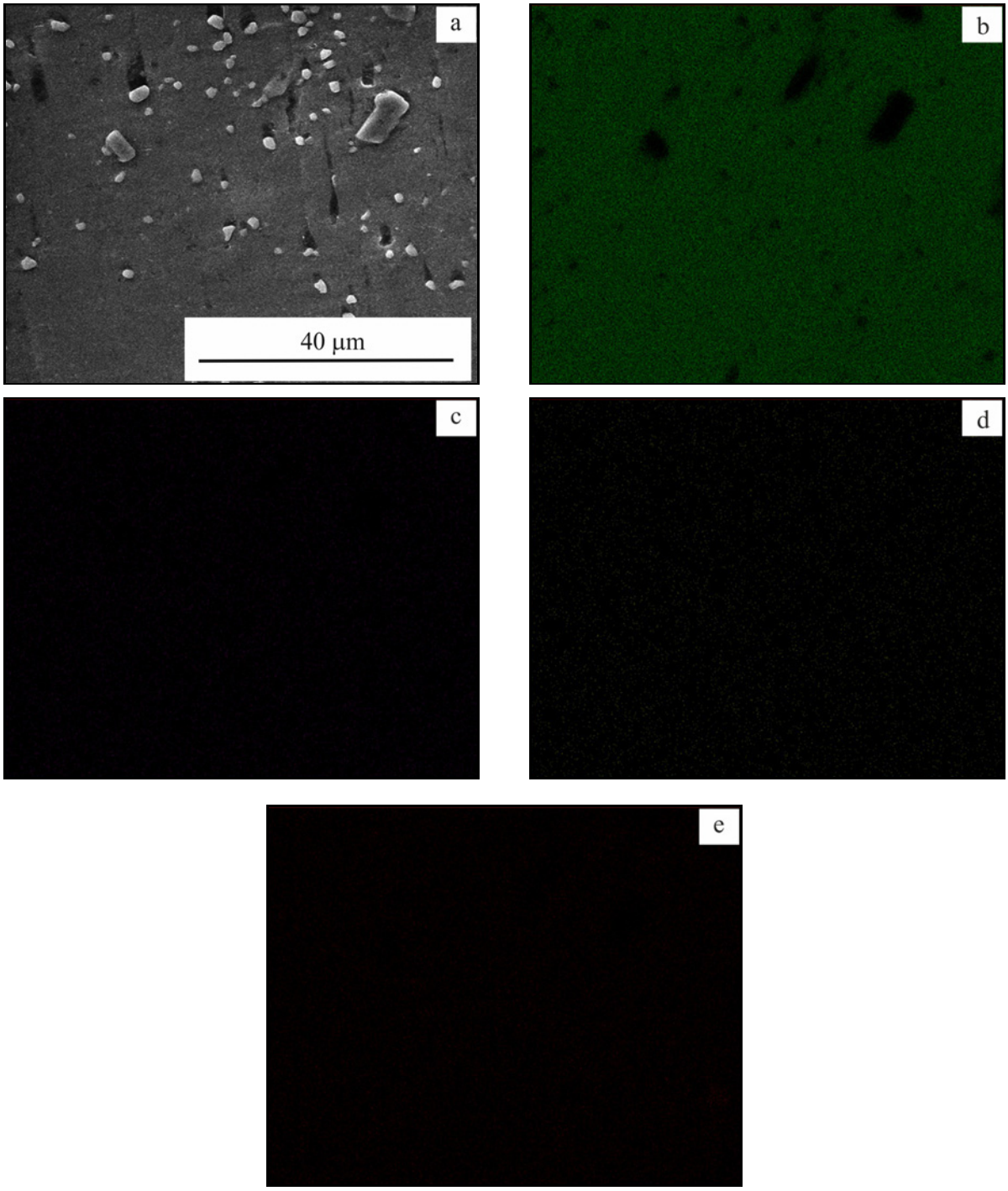

Fig. 8. Dispersion of elements in the AA-5TiB_2 composite, peak-aged at 120 °C: a) the composite microstructure, (b) Al, (c) Zn, (d) Cu, and (e) Mg.

namely AA-5TiB_2 which was peak-aged at 120 °C. One can see that the distribution of alloying elements is homogeneous.

The BSE images for the peak-aged and annealed samples in the polished condition are shown in Figs. 9 and 10, successively. For both kinds of sample groups concerning the thermal treatment, the secondary phase regions, which appear as white or light-colored in the matrix, are seen. In the annealed samples, the formation of coarse secondary phase particles is obtained to be more extensive compared to that in the peak-aged ones. Figure 11 reflects the EDX analyses of some locations in the annealed samples of AA-5TiB_2 and AA-10TiB_2. The second phase regions are found to be rich in alloying elements: Zn, Mg, and Cu.

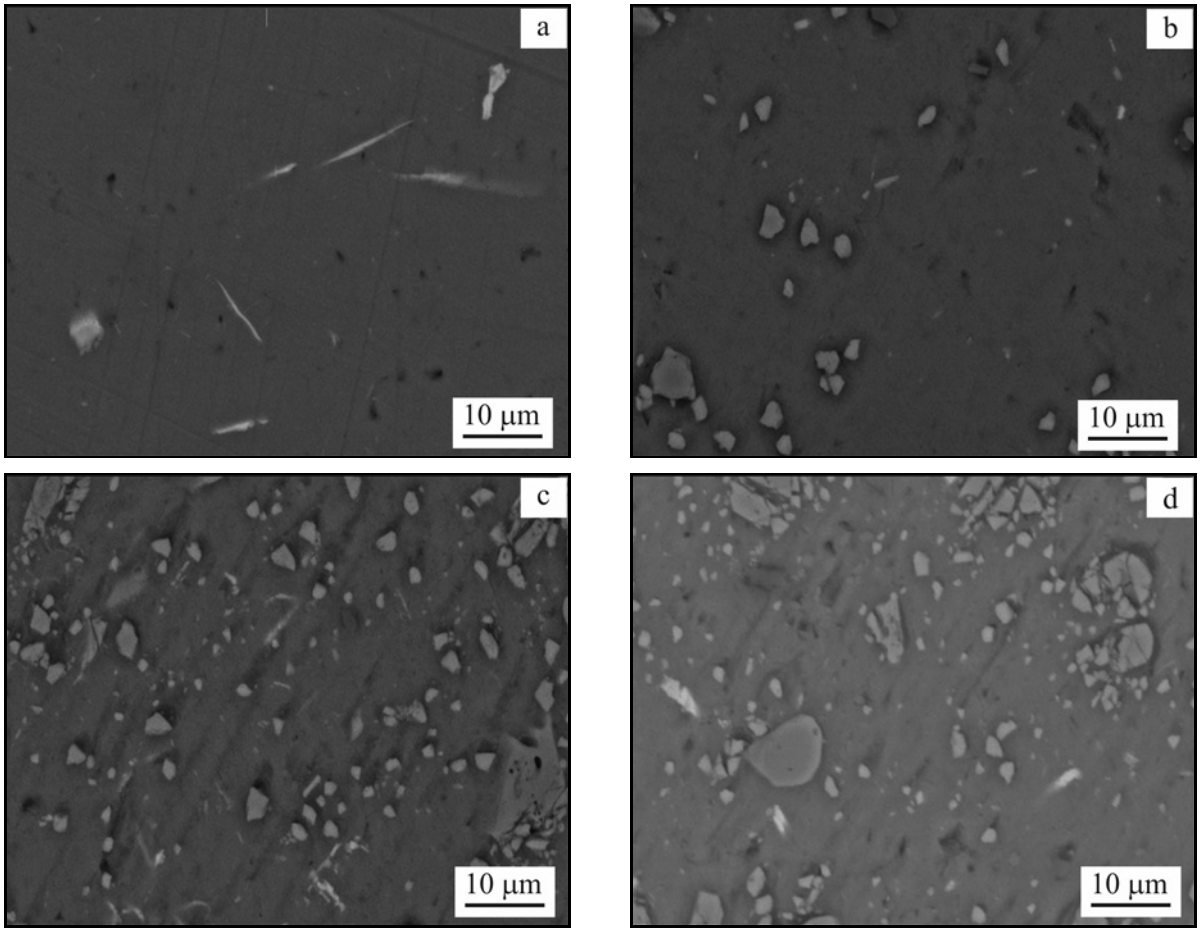

Fig. 9. The BSE images of the composite that was peak-aged at 120 °C: (a) AA, (b) AA-5TiB_2, (c) AA-10TiB_2, and (d) AA-15TiB_2 (3000 ×).

The XRD patterns for the artificially peak-aged and annealed samples are illustrated in Figs. 12 and 13, respectively. In addition to the main constituents of the samples, namely Al (ICSD no: 240129) and TiB_2 (ICSD no: 189387) [76], the intermetallic phases which are precipitated as $MgZn_2$ (ICSD no: 108587), MgZn (ICSD no: 151402), Al_2Cu (ICSD no: 151384), AlCuMg (ICSD no: 607006), $AlMg_4Zn_{11}$ (ICSD no: 57967), and Al_2CuMg (ICSD no:415062) are seen in the aged and annealed samples apparently [76]. Also, the oxides TiO_2 (ICSD no: 33844) and Ti_3O_5 (ICSD no: 75193) are detected in the annealed composites at a low scale [76]. The variation in these components' intensities depending on the TiB_2 ratio appears to be regular, as seen in the XRD analyses. The patterns indicate no Al_3Ti occurrence in the samples during the production and the heat treatment processes. This means that the use of cold compaction and sintering method in such composites obstructed the Al_3Ti formation. Tjong and Wang [54] reported that the Al_3Ti formation caused the reductions in the fatigue and tensile strength of the aluminum composites reinforced with TiB_{2p}.

3.4. Mechanical properties

The alloy, chosen as the matrix in this research, is sensible to heat treatment which means that it can be hardened substantially with precipitation heat treatment [65, 84–93]. The precipitation route from supersaturated solid solution (SSSS) for this alloy is expressed as follows [65, 84–94]:

$$\text{SSSS} \rightarrow \text{GP-I zones} \rightarrow \text{GP-II zones} \rightarrow \eta' \text{ (metastable } MgZn_2\text{)} \rightarrow \eta \text{ (stable } MgZn_2\text{)}. \quad (5)$$

In the above sequence, the supersaturated solid solution, formed after quenching from solutionizing treatment, initially transforms to GP-I zones which contain vacancy-rich clusters [84–91]. These zones and clusters turn into coherent GP-II zones that are precursors to the formation of η' phase, metastable $MgZn_2$ [84–91]. The η' precipitates, which are considered responsible for the maximum hardness and strength in the peak-aged condition of 7000 series of aluminum alloys, convert to stable and incoherent η phase if aging time is prolonged sufficiently [84–91].

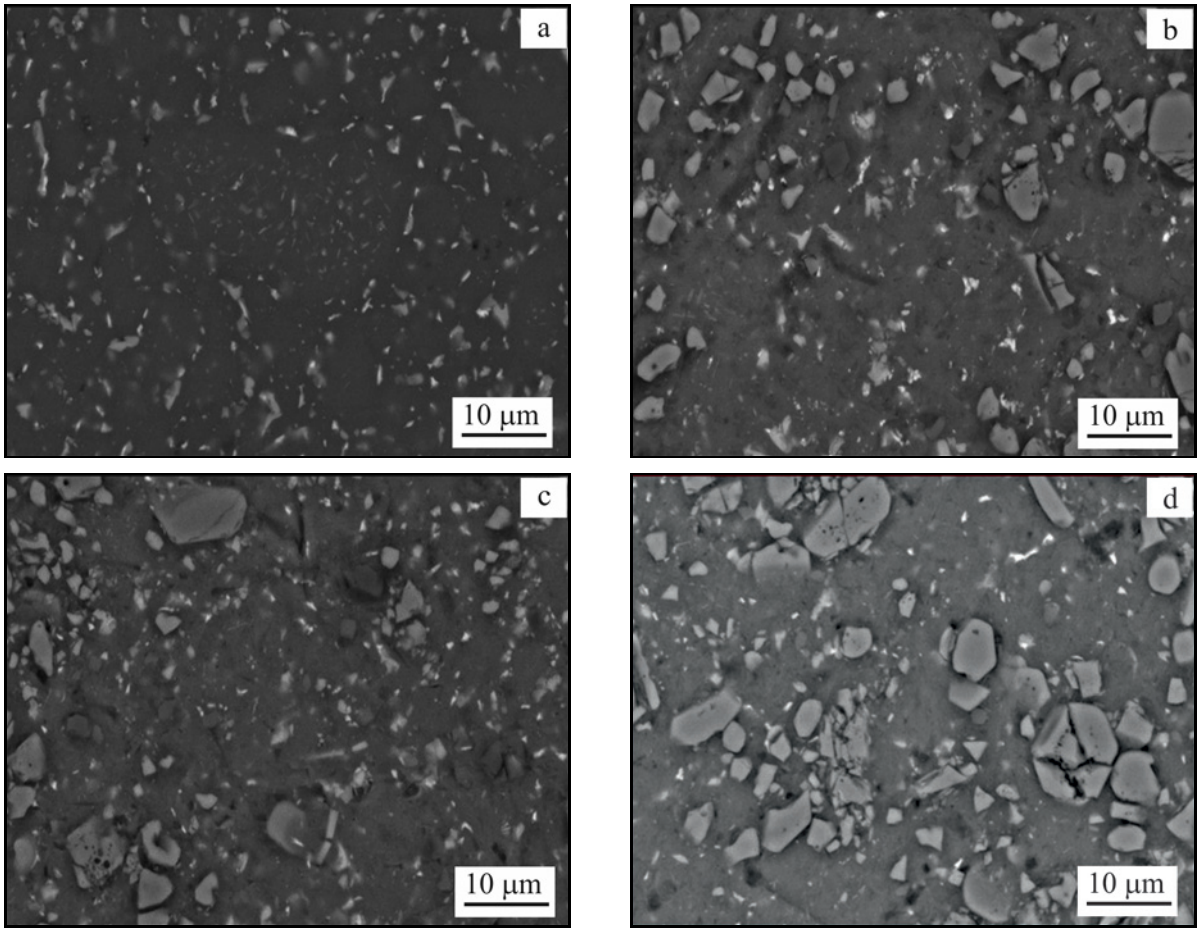

Fig. 10. The BSE pictures of the annealed composite: (a) AA, (b) AA-5TiB_2, (c) AA-10TiB_2, and (d) AA-15TiB_2 (3000 ×).

During overaging, the precipitates begin to grow in size. The incoherency between the η phase and aluminum solid solution is destroyed so that the hardness and strength of the alloy are decreased gradually with aging time [84–91].

The hardness change with respect to the aging period at 100 ℃ is shown in Fig. 14 for the produced materials. At starting, all samples' hardness values are very low, and they increase very rapidly in the first five hours. The maximum hardness was recorded to be 142 Brinell for the unreinforced aluminum alloy. In the meantime, the peak Brinell hardness values at the aging of 100 ℃, increasing with the reinforcement fraction, are obtained to be 148, 160, and 169 for the composites reinforced with 5, 10, and 15 % TiB_2, successively. After the peak aging, the hardness values begin to decrease and finally remain almost constant during the aging period of 25–100 h. The aging curves, derived at 120 ℃, are depicted in Fig. 15. The highest hardness values at this temperature are attained for the samples after an aging period of ∼ 11 h. They are 165, 184, 189, and 197 Brinell for the aluminum alloy reinforced with 0, 5, 10, and 15 % TiB_2, respectively. The profiles of the variation in hardness with aging time are similar for the examined materials. Moreover, the aging treatment's temporal hardness variations at 140 ℃ are represented in Fig. 16. The peak hardening for all materials obtained at this temperature is bigger than that at 100 ℃ but smaller than that at 120 ℃. Also, the lowest hardness values belong to the samples aged at 140 ℃ for 100 h. The precipitation kinetics of the PM composites bearing different amount of TiB_2 particles is found to trace similar paths with the unreinforced aluminum alloy. Therefore, the aging behavior of the Al-6.2Zn2.3Mg2.3Cu alloy is not altered upon the addition of TiB_2 particulates up to 15 vol.%.

It was previously stated that the precipitation kinetics was affected by augmentation of the dislocations throughout the matrix owing to the thermal incompatibility between ceramic reinforcement and metallic matrix [95–99]. The higher dislocation density, which created more nucleation zones for the precipitates, brought the acceleration of the matrix hardening of composites [95–99]. In other words, shorter times to reach peak hardness levels for the ceramic particle reinforced composites were required compared to the monolithic matrix [95–99]. Nevertheless, some other

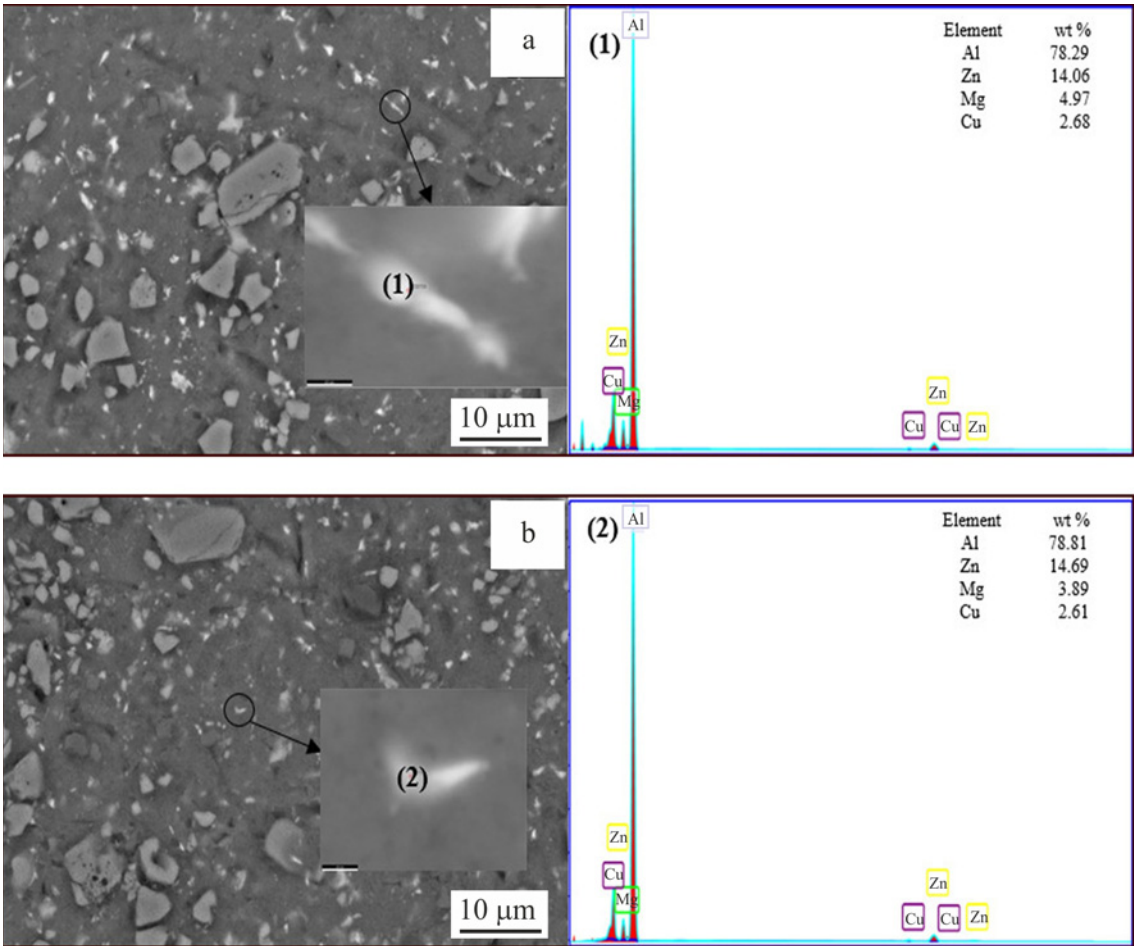

Fig. 11. The EDX analyses of some secondary phase regions in the annealed materials: (a) AA-5TiB_2 and (b) AA-10TiB_2.

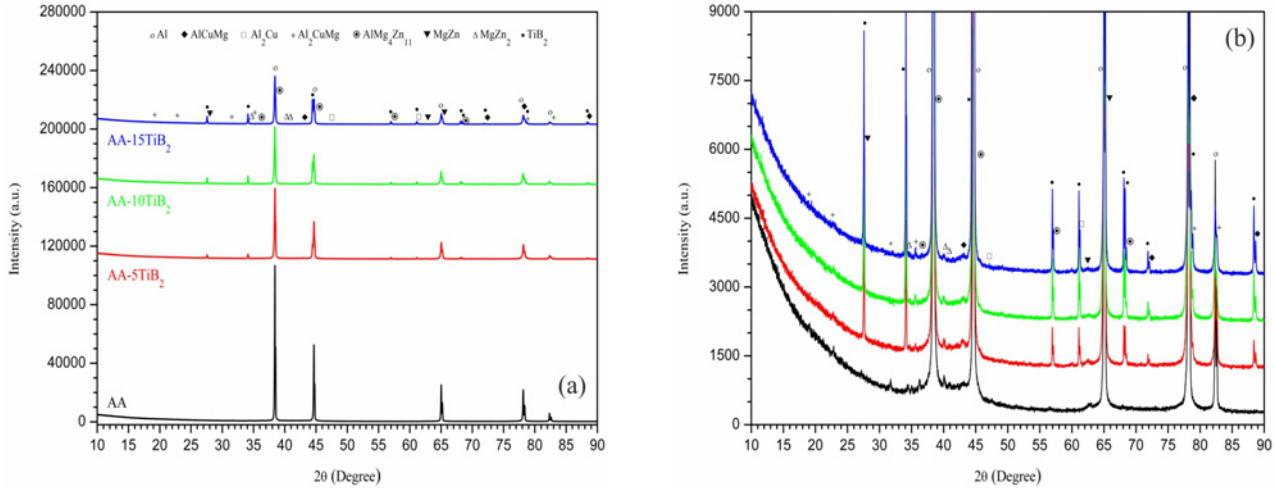

Fig. 12. The XRD patterns of the peak-aged specimens at 120 °C.

studies [100–106] showed different results about the peak-aging periods of aluminum composites compared to those of unreinforced aluminum alloys.

In the studies conducted on the Al-Mg-Cu/SiC_p [100] and AA2024/Al_2O_3 [101] composites, the addition of ceramic particulates entailed the slower aging kinetics and so lower peak aging periods concerning the unreinforced alloy. Furthermore, the period for reaching maximum hardness for the AA2024 composites reinforced with 20 % SiC_p was found to be higher

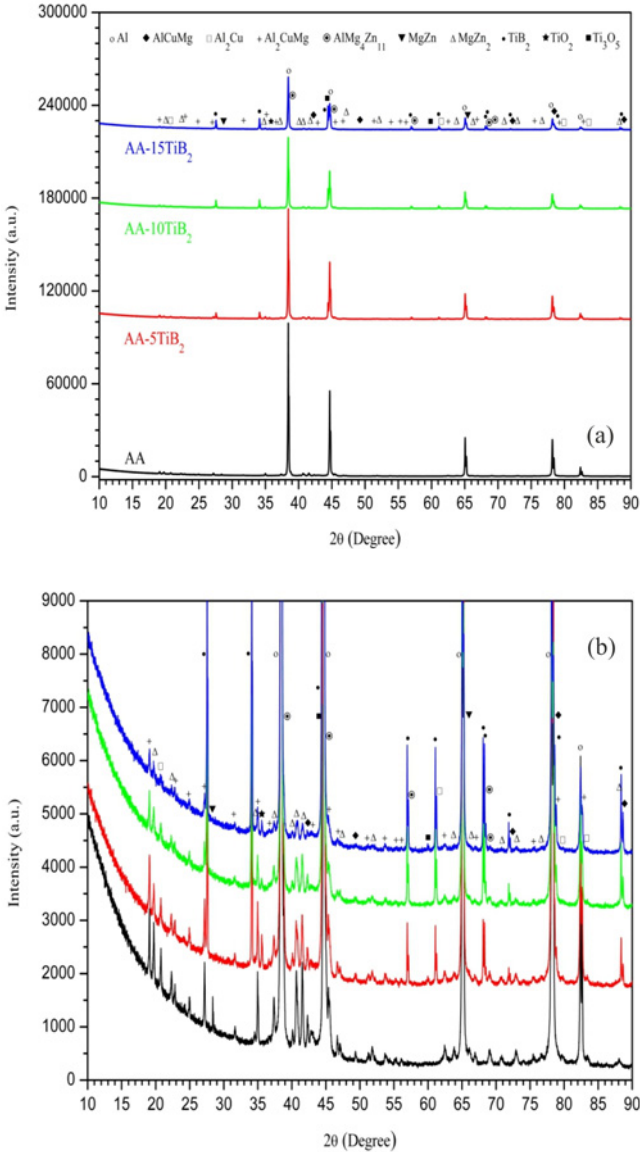

Fig. 13. The XRD results for the annealed specimens.

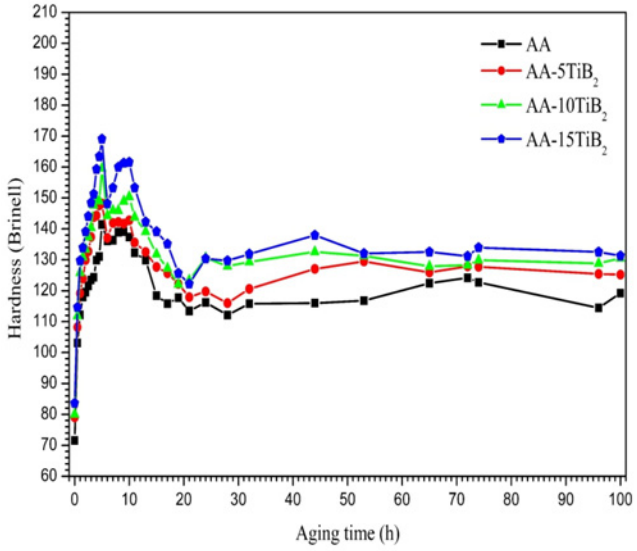

Fig. 14. The precipitation hardening curves for the investigated materials aged at 100 °C.

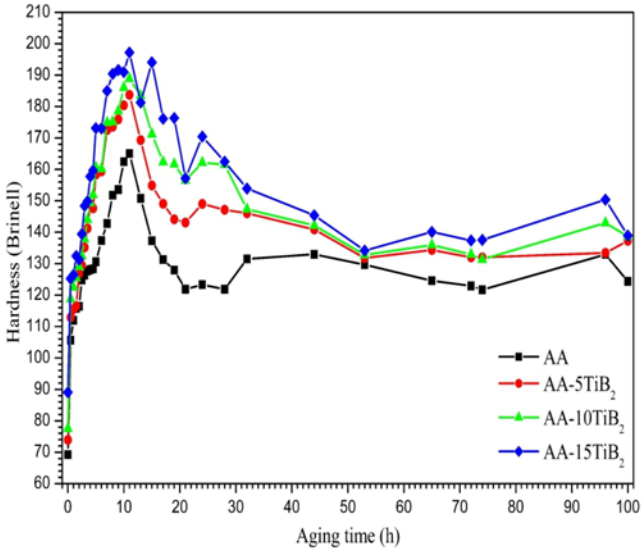

Fig. 15. The precipitation hardening profiles for the investigated materials aged at 120 °C.

than that for AA2024 alloy after the implementation of solutionizing at 495 ℃ for 1 h and artificial aging at 191 ℃ [102]. Moreover, the hardness variations with respect to aging time for composites were found to have a similar propensity with respect to those of unreinforced aluminum alloy in some studies [103–106]. In the current work, the main reason for having no change in the precipitation kinetics of composites with respect to that of AA could be related to lower dislocation density formation upon cooling from the solutionizing treatment [100, 101]. Therefore, the precipitation sites could not be increased sufficiently to fasten the aging process in the AA-TiB_2 composites [95–101].

The Brinell hardness was measured to be 48, 53, 54, and 55 for the annealed specimens, AA, AA-5, AA-10, and AA-15, respectively. The hardness levels of the annealed samples are much lower than those of aged ones, as expected since the coarse precipitate formation and the softening of the microstructure [65] in all the investigated samples occur. In a previous study by Singh et al. [62], a reduction in AA2014/TiB_2 composites' hardness was observed while the amount of TiB_2 was increased. They found the highest hardness of 138 VHN for the composite reinforced with 5 % TiB_2 after aging, while the lowest one was ∼ 105 VHN recorded for that with 15 % TiB_2 [62]. Moreover, only the AA2014 – 5 % TiB_2 composite had a

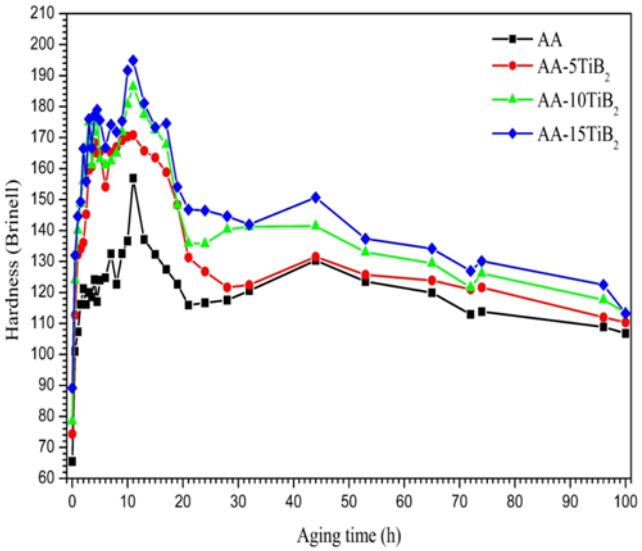

Fig. 16. Temporal hardness variation for the investigated materials aged at 140 °C.

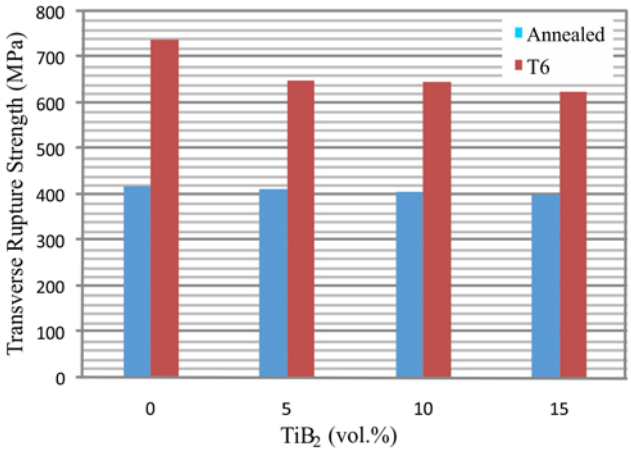

Fig. 17. The bending strength levels for the peak aged at 120 °C and annealed samples.

higher hardness than AA2014 [62]. In the current research, all samples' hardness levels are obtained to increase gradually as TiB_2 content increases at all aging temperatures. This means that the contribution of very hard TiB_2 particles [6–8] on the hardening of Al-6.2Zn2.3Mg2.3Cu alloy is taken place effectively due to the uniform structure formation except for some local ceramic clusters.

The TRS levels for the artificially aged and annealed samples are presented in Fig. 17. The artificially aged specimens have substantially higher strength than the annealed ones, as expected. Nevertheless, the incorporation of micron-sized TiB_2 particles results in lower TRS values, particularly in the aged samples. The highest TRS values are attained

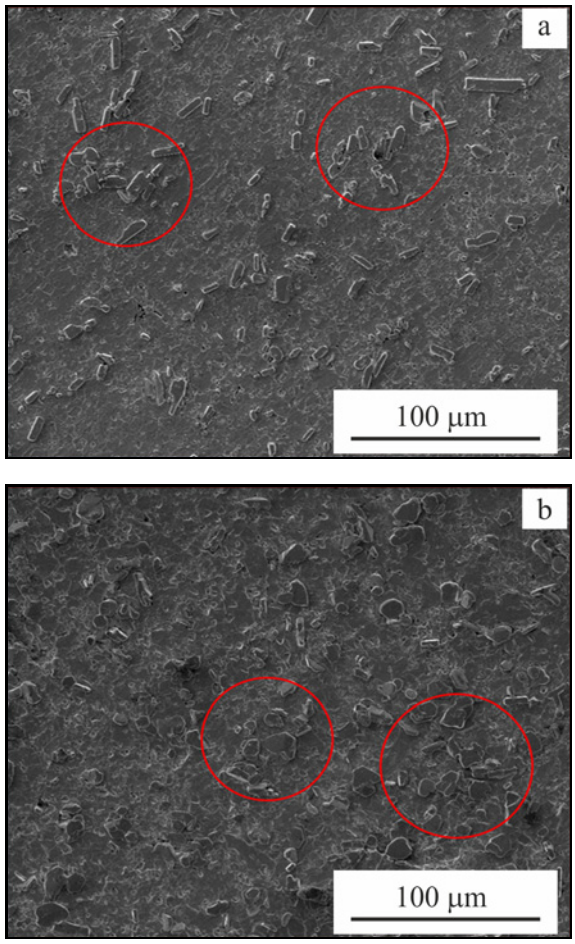

Fig. 18. Local particulate agglomeration in the composites with (a) 10 % TiB_2 and (b) 15 % TiB_2 (1000 ×).

for the aluminum alloy in both conditions. This is mainly attributed to the higher volumetric proportions of pores and some local agglomerations of TiB_2 particulates with increasing the TiB_2 fraction. Figure 18 demonstrates the characteristic formation of particle clusters locally for the composites with 10 and 15 % TiB_2.

It is well-known that pores' existence in the composites decreases the cross-sectional area and degrades the mechanical properties [58, 62, 70, 107–111]. Moreover, the local particle agglomeration leads to non-uniformity in composites' structure, affecting deformation and failure mechanisms [107, 112–117]. It locally brings about inhomogeneous deformation under the applied tensile stress on composites by creating high triaxial stresses on the matrix around the clusters of ceramic particles [107, 112–117]. These stresses enhance the initiation and linkage of voids in the matrix that lead to the fracture more easily [107, 112–117].

The TRS varies between 624 and 739 MPa for the peak aged samples, while it ranges between 401 and 417 MPa for the annealed samples depending on

the TiB_2 fraction. The small differences in the bending strength of the annealed samples are due to the higher plastic deformation ability of the softer matrix compared to the peak-aged ones. A similar trend in the TRS of the composites produced by cold pressing and sintering concerning TiB_2 particle content was also recorded for the AA2014/TiB_2 [62] or the AA6061/TiB_2 composites [58] recently. The TRS was reported to be ∼ 229 MPa for the aluminum alloy 2014, whereas it sharply decreased to ∼ 62 MPa for AA2014-15%TiB_2 composite [62]. In the other study [58], it was stated that even though the utilization of 5 % TiB_2 particle reinforcement in the alloy 6061 made a moderate improvement on the TRS, further additions of TiB_2 up to 15 % lowered it remarkably compared to the alloy 6061 [58]. The TRS values were obtained in the range of ∼ 140–180 MPa for the AA6061/TiB_2 composites using premixed alloy powder [58].

4. Conclusions

The main conclusions related to the experimental data gathered in this work can be outlined as below:

– The compressibility and density of the composite declined as its TiB_2 fraction increased.

– The densification of the powders during the cold pressing was almost completed at the compaction pressure of ∼ 600 MPa. Besides, the available compaction equations [66–68] worked very well with our data regarding the compressibility of the investigated powders.

– The dispersion of ceramic particles in the Al-6.2Zn2.3Mg2.3Cu alloy composites was usually obtained to be relatively uniform.

– The maximum hardness levels of all samples were reached at the aging of 120 ℃ after the period of ∼ 11 h.

– The precipitation hardening curves of the composites followed similar paths with the alloy so that the precipitation mechanism was not affected by the incorporation of TiB_2 particles.

– The TRS of the materials declined with the increasing TiB_2 ratio, somewhat more or less depending on the reinforcement content and heat treatment. Nonetheless, they were found to be much higher than the PM composites AA2014/TiB_2 [62] or the AA6061/TiB_2 [58].

Acknowledgements

This study was endorsed by the Scientific Research Projects Unit (Project No: OKÜBAP-2018-PT3-011) of Osmaniye Korkut Ata University. The authors are thankful to Osmaniye Korkut Ata University for funding the research.

References

[1] W. D. Callister, D. G. Rethwisch, Materials Science and Engineering, John Wiley and Sons, Inc. USA, 2011.

[2] F. L. Matthews, R. D. Rawlings, Composite Materials: Engineering and Science, Woodhead Publishing Limited and CRC Press LLC, 1999.

[3] N. Chawla, K. K. Chawla, Metal Matrix Composites, Springer Science & Business Media, New York, USA, 2013.

[4] K. U. Kainer, Basics of Metal Matrix Composites, In: K. U. Kainer (Ed.), Metal Matrix Composites: Custom-made Materials for Automotive and Aerospace Engineering, WILEY-VCH Verlag GmbH & Co. KGaA, Weinheim, 2006, pp. 1–54.

[5] H. Dieringa, K. U. Kainer, Particles, Fibers and Short Fibers for the Reinforcement of Metal Materials, In: K. U. Kainer (Ed.), Metal Matrix Composites: Custom-made Materials for Automotive and Aerospace Engineering, WILEY-VCH Verlag GmbH & Co. KGaA, Weinheim, 2006, pp. 55–76.

[6] V. I. Matkovich, Boron and Refractory Borides, Springer Verlag, New York, USA, 1977.

[7] R. G. Munro, Material properties of titanium diboride, J. Res. Natl. Inst. Stan. 105 (2000) 709–720. doi:10.6028/jres.105.057

[8] J. Besson, F. Valin, P. Lointier, M. Boncoeur, Densification of titanium diboride by hot isostatic pressing and production of near-net-shape components, J. Mat. Eng. Perf. 1 (1992) 637–650. doi:10.1007/BF02649245

[9] J. Geng, T. Hong, Y. Ma, M. Wang, D. Chen, N. Ma, H. Wang, The solution treatment of in-situ submicron TiB_2/2024 Al composite, Mater. Design 98 (2016) 186–193. doi:10.1016/j.matdes.2016.03.024

[10] K. Niranjan, P. R. Lakshminarayanan, Dry sliding wear behaviour of in-situ Al-TiB_2 composites, Mater. Design 47 (2013) 167–173. doi:10.1016/j.matdes.2012.11.035

[11] A. Mandal, M. Chakraborty, B. S. Murty, Effect of TiB_2 particles on sliding wear behaviour of Al-4Cu alloy, Wear 262 (2007) 160–166. doi:10.1016/j.wear.2006.04.003

[12] Y. Xiong, W. Wang, R. Jiang, K. Lin, G. Song, Surface integrity of milling in-situ TiB_2 particle reinforced Al matrix composites, Int. J. Refract. Met. H. 54 (2016) 407–416. doi:10.1016/j.ijrmhm.2015.09.007

[13] S. Agrawal, A. K. Ghose, I. Chakrabarty, Effect of rotary electromagnetic stirring during solidification of in-situ Al-TiB_2 composites, Mater. Design 113 (2017) 195–206. doi:10.1016/j.matdes.2016.10.007

[14] Z. Chen, G. A. Sun, Y. Wu, M. H. Mathon, A. Borbely, D. Chen, G. Ji, M. I. Wang, S. Y. Zhong, H. W. Wang, Multi-scale study of microstructure evolution in hot extruded nano-sized TiB_2 particle reinforced aluminum composites, Mater. Design 116 (2017) 577–590. doi:10.1016/j.matdes.2016.12.070

[15] A. Mandal, M. Chakraborty, B. S. Murty, Ageing behavior of A356 alloy reinforced with in-situ formed TiB_2 particles, Mat. Sci. Eng. A 489 (2008) 220–226. doi:10.1016/j.msea.2008.01.042

[16] K. Sivaprasad, S. P. K. Babu, S. Natarajan, R. Narayanasamy, B. A. Kumar, G. Dinesh, Study on abrasive and erosive wear behaviour of Al 6063/TiB_2

in situ composites, Mat. Sci. Eng. A 498 (2008) 495–500. doi:10.1016/j.msea.2008.09.003
[17] Q. Gao, S. Wu, S. Lü, X. Xiong, R. Du, P. An, Effects of ultrasonic vibration treatment on particles distribution of TiB_2 particles reinforced aluminum composites, Mat. Sci. Eng. A 680 (2017) 437–443. doi:10.1016/j.msea.2016.10.103
[18] Q. Gao, S. Wu, S. Lü, X. Xiong, R. Du, P. An, Improvement of particles distribution of in-situ 5 vol.% TiB_2 particulate reinforced Al-4.5Cu alloy matrix composites with ultrasonic vibration treatment, J. Alloy Compd. 692 (2017) 1–9. doi:10.1016/j.jallcom.2016.09.013
[19] U. A. Atturan, S. H. Nandam, B. S. Murty, S. Sankaran, Deformation behaviour of in-situ TiB_2 reinforced A357 aluminium alloy composite foams under compressive and impact loading, Mat. Sci. Eng. A 684 (2017) 178–185. doi:10.1016/j.msea.2016.12.048
[20] J. Nampoothiri, R. S. Harini, S. K. Nayak, B. Raj, K. R. Ravi, Post in-situ reaction ultrasonic treatment for generation of Al-4.4Cu/TiB_2 nanocomposite: A route to enhance the strength of metal matrix nanocomposites, J. Alloy Compd. 683 (2016) 370–378. doi:10.1016/j.jallcom.2016.05.067
[21] S. Thadela, B. Mandal, P. Das, H. Roy, A. K. Lohar, S. K. Samanta, Rheological behavior of semi-solid TiB_2 reinforced Al composite, T. Nonferr. Metal Soc. 25 (2015) 2827−2832. doi:10.1016/S1003-6326(15)63908-5
[22] J. Geng, T. Hong, Y. Shen, G. Liu, C. Xia, D. Chen, M. Wang, H. Wang, Microstructural stability of in-situ TiB_2/Al composite during solution treatment, Mater. Charact. 124 (2017) 50–57. doi:10.1016/j.matchar.2016.11.032
[23] X. Zhang, J. Sun, M. Wang, Y. Zhang, N. Ma, H. Wang, Improvement of yttrium on the hot tearing susceptibility of 6TiB_2/Al-5Cu composite, J. Rare Earth 33 (2015) 1335–1340. doi:10.1016/S1002-0721(14)60566-4
[24] Y. Ma, Z. Chen, M. Wang, D. Chen, N. Ma, H. Wang, High cycle fatigue behavior of the in-situ TiB_2/7050 composite, Mat. Sci. Eng. A 640 (2015) 350–356. doi:10.1016/j.msea.2015.06.023
[25] G.-S. Gan, B. Yang, Microstructure evolution of TiB_2 particle-reinforced 7075 Al alloy slurry in semisolid state with different holding time, Rare Metals 35 (2016) 858–862. doi:10.1007/s12598-015-0639-6
[26] H. B. M. Rajan, S. Ramabalan, I. Dinaharan, S. J. Vijay, Synthesis and characterization of in situ formed titanium diboride particulate reinforced AA 7075 aluminum alloy cast composites, Mater. Design 44 (2013) 438–445. doi:10.1016/j.matdes.2012.08.008
[27] S. Lakshmi, L. Lu, M. Gupta, In situ preparation of TiB_2 reinforced Al based composites, J. Mater. Process Tech. 73 (1998), 160–166. doi:10.1016/S0924-0136(97)00225-2
[28] T. Hong, X. Li, H. Wang, D. Chen, K. Wang, Effects of TiB_2 particles on aging behavior of in-situ TiB_2/Al-Cu-Mg composites,Mat. Sci. Eng. A 624 (2015) 110–117. doi:10.1016/j.msea.2014.11.072
[29] F. Wang, N. Ma, Y. Li, X. Li, H. Wang, Impact behavior of in situ TiB_2/Al composite at various temperatures, J. Mater. Sci. 46 (2011) 5192–5196. doi:10.1007/s10853-011-5454-3
[30] G. Gan, B. Yang, B. Zhang, X. Jiang, Y. Shi, Y. Wu, Refining mechanism of 7075 Al alloy by in-situ TiB_2 particles, Materials 10 (2017) 132. doi:10.3390/ma10020132
[31] S. Ji, F. Amirkhanlub, A. Mostaed, R. Beanland, Atomic structure and interface chemistry in a high-stiffness and high-strength Al-Si-Mg/TiB_2 nanocomposite, Mat. Sci. Eng. A 763 (2019) 138072. doi:10.1016/j.msea.2019.138072
[32] G. Liu, J. Geng, Y. Li, L. Cai, M. Wang, D. Chen, N. Ma, H. Wang, Effects of pre-strain on the microstructural evolution and mechanical strength of in situ TiB_2/7050 Al composite, Adv. Eng. Mater. 21 (2019) 1900042. doi:10.1002/adem.201900042
[33] S. L. Pramod, Ravikirana, A. K. Prasada Rao, B. S. Murty, Srinivasa R. Bakshi, Microstructure and mechanical properties of as-cast and T6 treated Sc modified A356-5TiB_2 in-situ composite, Mat. Sci. Eng. A 739 (2019) 383–394. doi:10.1016/j.msea.2018.10.080
[34] J. Xue, L. Zhang, J. Wang, R. Wan, Aging behavior of in-situ TiB_2 particles reinforced 2014Al alloy composites, Mater. Trans. 58 (2017) 33–38. doi:10.2320/matertrans.M2016146
[35] Y. Ma, A. Addad, G. Ji, M.-X. Zhang, W. Lefebvre, Z. Chen, V. Ji, Atomic-scale investigation of the interface precipitation in a TiB_2 nanoparticles reinforced Al-Zn-Mg-Cu matrix composite, Acta Mater. 185 (2020) 287–299. doi:10.1016/j.actamat.2019.11.068
[36] S. Mozammil, J. Karloopia, R. Verma, P. K. Jha, Effect of varying TiB_2 reinforcement and its ageing behaviour on tensile and hardness properties of in-situ Al-4.5%Cu-$x$$TiB_2$ composite, J. Alloy Compd. 793 (2019) 454–466. doi:10.1016/j.jallcom.2019.04.137
[37] S. M. Ma, P. Zhang, G. Ji, Z. Chen, G. A. Sun, S. Y. Zhong, V. Ji, H. W. Wang, Microstructure and mechanical properties of friction stir processed Al-Mg-Si alloys dispersion-strengthened by nanosized TiB_2 particles, J. Alloy Compd. 616 (2014) 128–136. doi:10.1016/j.jallcom.2014.07.092
[38] Ö. Balcı, D. Ağaoğulları, H. Gökçe, İ. Duman, M. L. Öveçoğlu, Influence of TiB_2 particle size on the microstructure and properties of Al matrix composites prepared via mechanical alloying and pressureless sintering, J. Alloy Compd. 586 (2014) 578–584. doi:10.1016/j.jallcom.2013.03.007
[39] Z. Sadeghian, B. Lotfi, M. H. Enayati, P. Beiss, Microstructural and mechanical evaluation of Al-TiB_2 nanostructured composite fabricated by mechanical alloying, J. Alloy Compd. 509 (2011) 7758–7763. doi:10.1016/j.jallcom.2011.04.145
[40] Z. Sadeghian, M. H. Enayati, P. Beiss, In-situ production of Al-TiB_2 nanocomposite by double-step mechanical alloying, J. Mater. Sci. 44 (2009) 2566–2572. doi:10.1007/s10853-009-3335-9
[41] D. Özyürek, İ. Çiftçi, An investigation into the wear behaviour of TiB_2 particle reinforced aluminium composites produced by mechanical alloying, Sci. Eng. Compos. Mater. 18 (2011) 5–12. doi:10.1515/SECM.2011.003
[42] E. Tekoğlu, D. Ağaoğulları, S. Mertdinç, M. L. Öveçoğlu, Effects of reinforcement content and sequential milling on the microstructural and mechanical properties of TiB_2 particulate-reinforced eutectic Al-12.6 wt.% Si composites, J. Mater. Sci. 53 (2018) 2537–2552. doi:10.1007/s10853-017-1687-0

[43] N. Abu-Warda, M. V. Utrilla, M. D. Escalera, E. Otero, M. D. López, The effect of TiB_2 content on the properties of AA6005/TiB_2 nanocomposites fabricated by mechanical alloying method, Powder Technol. 328 (2018) 235–244. doi:10.1016/j.powtec.2018.01.028

[44] M. K. Akbari, K. Shirvanimoghaddam, Z. Hai, S. Zhuiykov, H. Khayyam, Al-TiB_2 micro/nanocomposites: Particle capture investigations, strengthening mechanisms and mathematical modelling of mechanical properties, Mat. Sci. Eng. A 682 (2017) 98–106. doi:10.1016/j.msea.2016.11.034

[45] K. L. Tee, L. Lu, M. O. Lai, Synthesis of in situ Al-TiB_2 composites using stir cast route, Compos. Struct. 47 (1999) 589–593. doi:10.1016/S0263-8223(00)00030-1

[46] M. Karbalaei Akbari, H. R. Baharvandi, K. Shirvanimoghaddam, Tensile and fracture behavior of nano/micro TiB_2 particle reinforced casting A356 aluminum alloy composites, Mater. Design 66 (2015) 150–161. doi:10.1016/j.matdes.2014.10.048

[47] X. Dong, H. Youssef, Y. Zhang, S. Wang, S. Ji, High performance Al/TiB_2 composites fabricated by nanoparticle reinforcement and cutting-edge super vacuum assisted die casting process. Compos. Part B. 177 (2019) 107453. doi:10.1016/j.compositesb.2019.107453

[48] R. Krishna Kumar, N. Radhika, M. Sam, Synthesis of aluminium composites using squeeze casting and investigating the effect of reinforcements on their mechanical and wear properties, Trans. Indian Inst. Met. 72 (2019) 2299–2310. doi:10.1007/s12666-019-01680-6

[49] M. Askarpour, Z. Sadeghian, M. Reihanian, Role of powder preparation route on microstructure and mechanical properties of Al-TiB_2 composites fabricated by accumulative roll bonding (ARB), Mat. Sci. Eng. A 677 (2016) 400–410. doi:10.1016/j.msea.2016.09.068

[50] Ş. Ocak Araz, R. Çalın, M. Pul, O. Bican, O. Okur, An investigation on the microstructure and wear properties of TiB_2 reinforced AA2014 aluminium alloy produced by vacuum infiltration, High Temp. Mater. Proc. 34 (2015) 487–493. doi:10.1515/htmp-2014-0102

[51] S. C. Tjong, K. C. Lau, Properties and abrasive wear of TiB_2/Al-4%Cu composites produced by hot isostatic pressing, Compos. Sci. Technol. 59 (1999) 2005–2013. doi:10.1016/S0266-3538(99)00056-1

[52] S. C. Tjong, K. F. Tam, Mechanical and thermal expansion behavior of hipped aluminum-TiB_2 composites, Mater. Chem. Phys. 97 (2006) 91–97. doi:10.1016/j.matchemphys.2005.07.075

[53] H. Chi, L. Jiang, G. Chen, J. Qiao, X. Lin, G. Wu, The tribological behavior evolution of TiB_2/Al composites from running-in stage to steady state, Wear 368–369 (2016) 304–313. doi:10.1016/j.wear.2016.10.003

[54] S. C. Tjong, G. S. Wang, Y. W. Mai, High cycle fatigue response of in-situ Al-based composites containing TiB_2 and Al_2O_3 submicron particles, Compos. Sci. Technol. 65 (2005) 1537–1546. doi:10.1016/j.compscitech.2005.01.012

[55] T. Imai, G. L'esperance, B. D. Hong, Y. Tozawa, High strain rate superplasticity of TiB_2 particulate reinforced aluminium alloy composite, J. Mater. Sci. Lett. 14 (1995) 373–376. doi:10.1007/BF00592153

[56] P. H. Vajargah, H. Abdizadeh, M. A. Baghchesara, Fabrication of TiB_2 nano particulates reinforced aluminum matrix composites by powder metallurgy route, J. Compos. Mater. 49 (2015) 3115–3125. doi:10.1177/0021998314560382

[57] J. Oñoro, High-temperature mechanical properties of aluminium alloys reinforced with titanium diboride (TiB_2) particles, Rare Metals 30 (2011) 200–205. doi:10.1007/s12598-011-0224-6

[58] M. Paidpilli, G. K. Gupta, A. Upadhyaya, Sintering response of aluminum 6061-TiB_2 composite: Effect of prealloyed and premixed matrix, J. Mater. Eng. Perform. 26 (2017) 4470–4480. doi:10.1007/s11665-017-2883-4

[59] F. E. Başar, Production and characterization of aluminium matrix composites via pressureless sintering. M.Sc. Thesis, Akdeniz University Institute of Natural and Applied Sciences, Mechanical Engineering, Antalya, 2011 (in Turkish).

[60] M. Übeyli, D. Zalaoğlu, Natural aging behavior of composites containing a high-strength aluminum alloy matrix and titanium diboride particles, Proceedings of 3rd Metallurgical and Materials Engineering Congress of South-East Europe 2017, p. 23. ISBN 978-86-87183-29-2

[61] N. Kumar, G. Gautam, R. K. Gautam, A. Mohan, S. Mohan, Synthesis and characterization of TiB_2 reinforced aluminum matrix composites: A review, J. Inst. Eng. India Ser. D 97 (2016) 233–253. doi:10.1007/s40033-015-0091-7

[62] R. P. Singh, G. K. Gupta, M. Paliwal, An experimental and modeling study of synthesis, consolidation and aging behavior of AA2014 composite reinforced by TiB_2 via powder metallurgy route, Trans. Indian Inst. Met. 71 (2018) 2443–2451. doi:10.1007/s12666-018-1375-z

[63] S. Suresh, A. Mortensen, A. Needleman, Fundamentals of Metal Matrix Composites, Butterworth-Heinemann, Oxford, 1993.

[64] Y. B. Liu, S. C. Lim, L. Lu, M. O. Lai, Recent development in the fabrication of metal matrix-particulate composites using powder metallurgy techniques, J. Mater. Sci. 29 (1994) 1999–2007. doi:10.1007/BF01154673

[65] J. R. Davis, ASM Specialty Handbook, Aluminum and Aluminum Alloys, ASM International, USA, 1993.

[66] R. W. Heckel, Density-pressure relationships in powder compaction, T. Metall. Soc. AIME 221 (1961) 671–675.

[67] R. Ge, A new equation for powder compaction, Powder Metall. Sci. Technol. 6 (1995) 20–24.

[68] R. Panelli, F. Ambrozio Filho, Compaction equation and its use to describe powder consolidation behavior, Powder Metall. 41 (1998) 131–133. doi:10.1179/pom.1998.41.2.131

[69] R. Panelli, F. Ambrozio Filho, A study of a new phenomenological compacting equation, Powder Technol. 114 (2001) 255–261. doi:10.1016/S0032-5910(00)00207-2

[70] R. M. German, Powder Metallurgy & Particulate Materials Processing, Metal Powder Industries Federation, Princeton, New Jersey, USA, 2005.

[71] ASTM B962-17: Standard test methods for density of compacted or sintered powder metallurgy (PM) products using Archimedes' principle, 2017.

[72] ASTM E10-17: Standard Test Method for Brinell Hardness of Metallic Materials, 2017.
[73] George F. Vander Voort, Metallography: Principles and Practice, ASM International, New York, 1999.
[74] T. Degen, M. Sadki, E. Bron, U. König, G. Nénert, The High Score suite, Powder Diffr. 29 S2 (2014) S13–S18. doi:10.1017/S0885715614000840
[75] HighScore Software Program, Malvern Panalytical, https://www.malvernpanalytical.com/en/products/category/software/x-ray-diffraction-software/highscore/, 2020 (accessed 24 February 2020).
[76] Inorganic Crystal Structure Database (ICSD) ,Fachinformationszentrum (FIZ), Karlsruhe, Germany, 2016.
[77] TS 4222 EN ISO 3325. Sintered metal materials, excluding hard metals -Determination of transverse rupture strength (in Turkish), 2004.
[78] D. Bouvard, Densification behaviour of mixtures of hard and soft powders under pressure, Powder Technol. 111 (2000) 231–239. doi:10.1016/S0032-5910(99)00293-4
[79] S. Mahdavi, F. Akhlaghi, Effect of SiC content on the processing, compaction behavior and properties of Al6061/SiC/Gr hybrid composites, J. Mater. Sci. 46 (2011) 1502–1511. doi:10.1007/s10853-010-4954-x
[80] P. J. Denny, Compaction equations: A comparison of the Heckel and Kawakita equations, Powder Technol. 127 (2002) 162–172. doi:10.1016/S0032-5910(02)00111-0
[81] H. R. Hafizpour, M. Sanjari, A. Simchi, Analysis of the effect of reinforcement particles on the compressibility of Al-SiC composite powders using a neural network model, Mater. Design 30 (2009) 1518–1523. doi:10.1016/j.matdes.2008.07.052
[82] W. Wu, G. Jiang, R. H. Wagoner, G. S. Daehn, Experimental and numerical investigation of idealized consolidation Part I: Static compaction, Acta Mater. 48 (2000) 4323–4330. doi:10.1016/S1359-6454(00)00206-8
[83] J. A. Lund, Origins of green strength in iron P/M compacts, Int. J. of Powder Metall. & Powder Technol. 18 (1982) 117–127.
[84] L. F. Mondolfo, N. A. Gjostein, D. W. Levinson, Structural changes during the aging in an Al-Mg-Zn alloy, Trans. AIME J. Metals 206 (1956) 1378–1385. doi:10.1007/BF03377889
[85] H. Löffler, I. Kovacs, J. Lendvai, Decomposition processes in Al-Zn-Mg alloys, J. Mat. Sci. 18 (1983) 2215–2240. doi:10.1007/BF00541825
[86] J. Gjønnes, Chr. J. Simesen, An electron microscope investigation of the microstructure in an aluminium-zinc-magnesium alloy, Acta Metall. Mater. 18 (1970) 881–890. doi:10.1016/0001-6160(70)90016-7
[87] L. F. Mondolfo, Structure of the aluminium: Zinc: magnesium alloys, Metallurgical Rev. 16 (1971) 95–124. doi:10.1179/mtlr.1971.16.1.95
[88] J. Lendvai, Precipitation and strengthening in aluminium alloys, Mater. Sci. Forum 217–222 (1996) 43–56. doi:10.4028/www.scientific.net/MSF.217-222.43
[89] G. Sha, A. Cerezo, Characterization of precipitates in an aged 7xxx series Al alloy, Surf. Interface Anal. 36 (2004) 564–568. doi:10.1002/sia.1702
[90] L. K. Berg, J. Gjonnes, V. Hansen, X. Z. Li, M. Knutson-Wedel, G. Waterloo, D. Schryvers, L. R. Wallenberg, GP zones in Al-Zn-Mg alloys and their role in artificial aging, Acta Mater. 49 (2001) 3443–3451. doi:10.1016/S1359-6454(01)00251-8
[91] A. Deschamps, Y. Brechet, F. Livet, Influence of copper addition on precipitation kinetics and hardening in Al-Zn-Mg alloy, Mater. Sci. Tech. 15 (1999) 993–1000. doi:10.1179/026708399101506832
[92] G. Sha, A. Cerezo, Early stage precipitation in Al-Zn--Mg-Cu alloy (7050), Acta Mater. 52 (2004) 4503–4516. doi:10.1016/j.actamat.2004.06.025
[93] L. F. Mondolfo, Aluminum Alloys: Structure and Properties, Butterworths, London, 1976.
[94] K. Stiller, P. J. Warren, V. Hansen, J. Angenete, J. Gjonnes, Investigation of precipitation in an Al-Zn--Mg alloy after two step ageing treatment at 100 °C and 150 °C, Mater. Sci. Eng. A 270 (1999) 55–63. doi:10.1016/S0921-5093(99)00231-2
[95] Z. M. El-Baradie, O. A. El-Shahat, A. N. Abd El-Azim, Accelerated aging processes in SiC-7020 aluminum composite, J. Mater. Process Tech. 79 (1998) 1–8. doi:10.1016/S0924-0136(97)00096-4
[96] R. J. Arsenault, N. Shi, Dislocation generation due to differences between the coefficients of thermal expansion, Mater. Sci. Eng. 81 (1986) 175–187. doi:10.1016/0025-5416(86)90261-2
[97] S. K. Varma, J. Ponce, M. Solis, S. Andrews, D. Salas, The control of grain size and distribution of particles in a $(6061\ \text{Alloy})_m/(Al_2O_3)_p$ composite by solutionizing treatment, Metall. Mater. Trans. A 27 (1996) 2023–2034. doi:10.1007/BF02651951
[98] I. Dutta, S. M. Allen, J. L. Hafley, Effect of the reinforcement on the aging response of cast 6061 Al-Al_2O_3 particulate composites, Metall. Trans. A 22 (1991) 2553–2563. doi:10.1007/BF02851349
[99] R. J. Arsenault, R. M. Fischer, Microstructure of fiber and particulate SiC in 6061 Al composites, Scripta Metall. Mater. 17 (1983) 67–71. doi:10.1016/0036-9748(83)90072-8
[100] S. Pal, R. Mitra, V. V. Bhanuprasad, Aging behavior of Al-Cu-Mg alloy – SiC composites, Mat. Sci. Eng. A 480 (2008) 496–505. doi:10.1016/j.msea.2007.07.072
[101] A. N. Abdel-Azim, Y. Shash, S. F. Mostafa, A. Younan, Ageing behaviour of 2024-Al alloy reinforced with Al_2O_3 particles, J. Mater. Process. Tech. 55 (1995) 140–145. doi:10.1016/0924-0136(95)01946-4
[102] S. M. R. Mousavi Abarghouie, S. M. Seyed Reihani, Aging behavior of a 2024 Al alloy-SiC_p composite, Mater. Design 31 (2010) 2368–2374. doi:10.1016/j.matdes.2009.11.063
[103] M. Übeyli, E. Balci, B. Sarikan, M. K. Öztaş, N. Camuşcu, R. O. Yildirim, Ö. Keleş, The ballistic performance of SiC-AA7075 functionally graded composite produced by powder metallurgy, Mater. Design 56 (2014) 31–36. doi:10.1016/j.matdes.2013.10.092
[104] E. Balcı, B. Sarıkan, M. Übeyli, N. Camuşcu, R. O. Yıldırım, On the ballistic performance of the AA7075 based functionally graded material with boron carbide reinforcement, Kovove Mater. 51 (2013) 257–262. doi:10.4149/km_2013_4_257
[105] C. Y. Sheu, S. J. Lin, Ageing behavior of SiC_p-reinforced AA 7075 composites, J. Mater. Sci. 32 (1997) 1741–1747. doi:10.1023/A:1018576000575
[106] L. Lu, M. O. Lai, F. L. Chen, Al-4 wt.% Cu composite reinforced with in-situ TiB_2 particles, Acta Mater. 45 (1997) 4297–4309. doi:10.1016/S1359-6454(97)00075-X

[107] T. W. Clyne, P. J. Withers, An Introduction to Metal Matrix Composites, Cambridge University Press, Cambridge, 1993.
[108] C. S. Kim, K. Cho, M. H. Manjili, M. Nezafati, Mechanical performance of particulate-reinforced Al metal-matrix composites (MMCs) and Al metal-matrix nano-composites (MMNCs), J. Mater. Sci. 52 (2017) 13319–13349. doi:10.1007/s10853-017-1378-x
[109] A. A. Mazen, A. Y. Ahmed, Mechanical behavior of Al-Al_2O_3 MMC manufactured by PM techniques Part I – Scheme I Processing parameters, J. Mater. Eng. Perform. 7 (1998) 393–401. doi:10.1361/105994998770347846
[110] C. P. Ling, M. B. Bush, D. S. Perera, The effect of fabrication techniques on the properties of A1-SiC composites, J. Mater. Process. Tech. 48 (1995) 325–331.
[111] H. R. Ezatpour, S. A. Sajjadi, M. H. Sabzevar, Y. Huang, Investigation of microstructure and mechanical properties of Al6061 nanocomposite fabricated by stir casting, Mater. Design 55 (2014) 921–928. doi:10.1016/j.matdes.2013.10.060
[112] D. J. Lloyd, Aspects of fracture in particulate reinforced metal matrix composites, Acta Metall. Mater. 39 (1991) 59–71. doi:10.1016/0956-7151(91)90328-X
[113] J. J. Lewandowski, C. Liu, W. H. Hunt Jr., Effects of matrix microstructure and particle distribution on fracture of an aluminum metal matrix composite, Mat. Sci. Eng. A 107 (1989) 241–255. doi:10.1016/0921-5093(89)90392-4
[114] A. F. Whitehouse, T. W. Clyne, Cavity formation during tensile straining of particulate and short fibre metal matrix composites, Acta Metall. Mater. 41 (1993) 1701–1711. doi:10.1016/0956-7151(93)90189-Y
[115] A. F. Whitehouse, T. W. Clyne, Effects of reinforcement content and shape on cavitation and failure in metal matrix composites, Composites 24 (1993) 256–261. doi:10.1016/0010-4361(93)90172-5
[116] J. Llorca, A. Needleman, S. Suresh, An analysis of the effects of matrix void growth on deformation and ductility in metal-ceramic composites, Acta Metall. Mater. 39 (1991) 2317–2335. doi:10.1016/0956-7151(91)90014-R
[117] T. Christman, A. Needleman, S. Suresh, An experimental and numerical study of deformation in metal-ceramic composites, Acta Metall. 37 (1989) 3029–3050. doi:10.1016/0001-6160(89)90339-8